

Tailoring Liquid/Solid Interfacial Energy Transfer: Fabrication and Application of Multiscale Metallic Surfaces With Engineered Heat Transfer and Electrolysis Properties Via Femtosecond Laser Surface Processing Techniques

Troy P. Anderson^a, Chris Wilson^a, Craig A. Zuhlke^a, Corey Kruse^b, Anton Hassebrook^b, Isra Somanas^b, Sidy Ndao^b, George Gogos^b, Dennis Alexander^a

^aDept. of Electrical Engineering, University of Nebraska – Lincoln, 209N Scott Engineering Center, Lincoln, NE USA 68588; ^bDept. of Mechanical and Materials Engineering, University of Nebraska – Lincoln, 209N Scott Engineering Center, Lincoln, NE USA 68588

*troy.anderson@unl.edu

ABSTRACT

Femtosecond Laser Surface Processing (FLSP) is a powerful technique for the fabrication of self-organized multiscale surface structures on metals that are critical for advanced control over energy transfer at a liquid/solid interface in applications such as electrolysis. The efficiency of the hydrogen evolution reaction on stainless steel 316 electrodes in a 1 molar potassium hydroxide solution is used to analyze the role of surface geometry to facilitate the phase conversion of the liquid to a gaseous state in the vicinity of the interface. It is found that the efficiency of the electrolysis process is directly related to the separation of micro-scale features on an electrode surface. The enhancement is attributed to the size of the valleys between microstructures controlling the contact between an evolving vapor bubble and the electrode surface. The results suggest an alternative pathway for the tailoring of interfacial energy transfer on structured surfaces separate from traditional benchmarks such as surface area and contact angle.

Keywords: Femtosecond Laser Surface Processing, Electrolysis, Bubble Overvoltage, Stainless Steel

1. INTRODUCTION

Femtosecond laser surface processing (FLSP) is rapidly emerging as a powerful technique for the fabrication of biologically inspired multiscale surface structures with highly-tailorable surface properties. Laser-processed surfaces generally consist of self-organized, quasi-periodic micron-scale conical or mound structures that are covered in a layer of nanoparticles [1-8]. These surface structures are formed through a complex combination of multiple growth mechanisms including laser ablation, capillary flow of laser-induced melt layers, and redeposition of ablated material. One of the most promising applications of multiscale surfaces is to enhance the efficiency of energy transfer during phase conversion at a surface; for example, boiling, condensation, and electrochemical gas evolution are all classic examples of such processes. The ability of a multiscale metallic surface to affect heat transfer has been previously described [9]. This paper describes the application of multiscale metallic surfaces to the generation of hydrogen gas via electrolysis in an alkaline cell, which is critically important for the development of a large-scale hydrogen production system. Water is split into hydrogen and oxygen gas in an electrolysis cell by driving a current between two electrodes immersed in an aqueous solution. The amount of hydrogen and oxygen gas generated is directly dependent on the current; for every four electrons passed through the cell, one O₂ molecule is formed at the anode and two H₂ molecules are formed at the cathode. The voltage required to pass a given current through the cell determines the efficiency of the cell, with the cell efficiency being inversely proportional to the voltage.

The interfacial energy transfer between a solid and an adjacent liquid is governed in part by the ability of a surface to facilitate the phase conversion of the liquid to a gaseous state in the vicinity of the interface. This phase conversion generally occurs at specific nucleation sites where bubbles grow and are eventually released when buoyancy, flow, or turbulence overcomes the adhesion between the bubble and the surface [10]. However, there exists a natural inefficiency in the process: the generation and growth of a gas bubble at a nucleation site covers a portion of the surface, which reduces contact with the solid surface and decreases the efficiency of the electrochemical reaction. It is desirable to simultaneously reduce the diameter of bubbles released from the surface and increase the release rate [11-13]. The current paper investigates the role of multiscale structures with micro- and nano-scale features on electrode surfaces as

an alternative approach to bubble mitigation and thus the enhancement of the phase transition efficiency. Specifically, the role of the separation distance between surface micro-scale structures on the electrolysis efficiency is investigated.

2. EXPERIMENT

2.1 Femtosecond Laser Surface Processing

Femtosecond laser surface processing (FLSP) is used to physically shape the surface profile of the electrode surfaces in order to provide enhanced performance. The laser used was a Ti:Sapphire laser (Spitfire, Spectra Physics) capable of producing 1 mJ, 50 fs pulses with a center wavelength of 800 nm at a repetition rate of 1 kHz. Laser characteristics such as the pulse length and chirp were monitored and optimized using a Frequency Resolved Optical Gating (FROG) instrument from Positive Light (Model 8-02). The schematic of the experimental setup has been previously published [1,2]. The impact of the surface morphology on the electrolysis efficiency was studied with a series of 6 distinct surface including 5 laser-processed surfaces and one unprocessed surface as a control. To generate laser-processed surface features, a target electrode was placed on a 3D computer-controlled translation stage and translated through a laser beam with a square flat-top profile with 150 μm sides. The flat top-profile was generated with a refractive beam shaper (GTH-4-2.2FA, Eksma Optics) in order to provide uniform laser fluence on the sample during processing. The laser fluence was varied from 1 – 2.9 J/cm² and the number of pulses per laser spot was held constant at 400 for all samples. Laser illumination was performed in ambient atmosphere. The resulting electrode surfaces are characterized by multiscale self-organized features on the order of 10-50 microns in height and width that are covered in a layer of nanoparticles that develop on the surface through a combination of growth mechanisms including preferential ablation, capillary flow of laser-induced melt layers, and redeposition of ablated surface features. In this range of laser parameters, the surfaces morphologies span from below surface growth mounds (BSG-mounds) to above surface growth mounds (ASG-mounds) [1,2,5]. Scanning electron microscope (SEM) images of the electrode surfaces as well as 3D surface profiles measured with a Keyence VK-X100 laser confocal scanning microscope are shown in Figure 1. The Keyence system has an axial resolution of 0.5 nm and a transverse resolution of 120 nm. The associated fabrication parameters and relevant surface characteristics for these surfaces are given in Table 1.

The average structure height, surface area ratio and surface roughness were determined by analysis of the 3D surface profile. The surface area ratio, commonly called the roughness factor, is the ratio of the total surface area to the geometric area. Due to the resolution limits of the Keyence system, the surface area ratio and the roughness factor do not consider any nanoparticles on the surface. Because the micro-scale structures are self-organized and are not uniformly spaced, the separation distance between surface structures was statistically calculated using a 2D Frequency Fourier Transform (FFT) analysis of the SEM images. The 2D FFT of plate 1 is characterized by a broad ring of spatial frequencies. The average structure spacing was calculated by averaging 50 angular slices of the 2D FFT and taking the peak value. The contact angle of a 1 μL water droplet on the sample was measured to be less than 5° for all laser-processed samples, indicating superhydrophilicity. This is advantageous in electrolysis as it enhances the contact between the electrode and the electrolyte. Furthermore, since all surfaces are superhydrophilic with indistinguishable contact angles, any variations of the performance of the electrodes can be attributed to differences in the geometric surface profile.

Table 1: Laser processing conditions and surface properties of stainless steel 316 electrode surfaces.

Design Parameters		Measured Parameters			
Sample Name	Laser Fluence [J/cm ²]	Average Height [μm]	Surface Area Ratio	Surface Roughness [μm Rrms]	Structure Separation [μm]
S1	1.0	12.4	4.2	1.5	6.1
S2	1.33	13.8	4.9	1.6	7.0
S3	2.0	8.3	4.2	3.8	12.2
S4	2.3	13.1	4.2	3.9	9.8
S5	2.5	10.3	4.8	3.0	12.3
S6	2.9	13.5	4.5	5.0	13.4

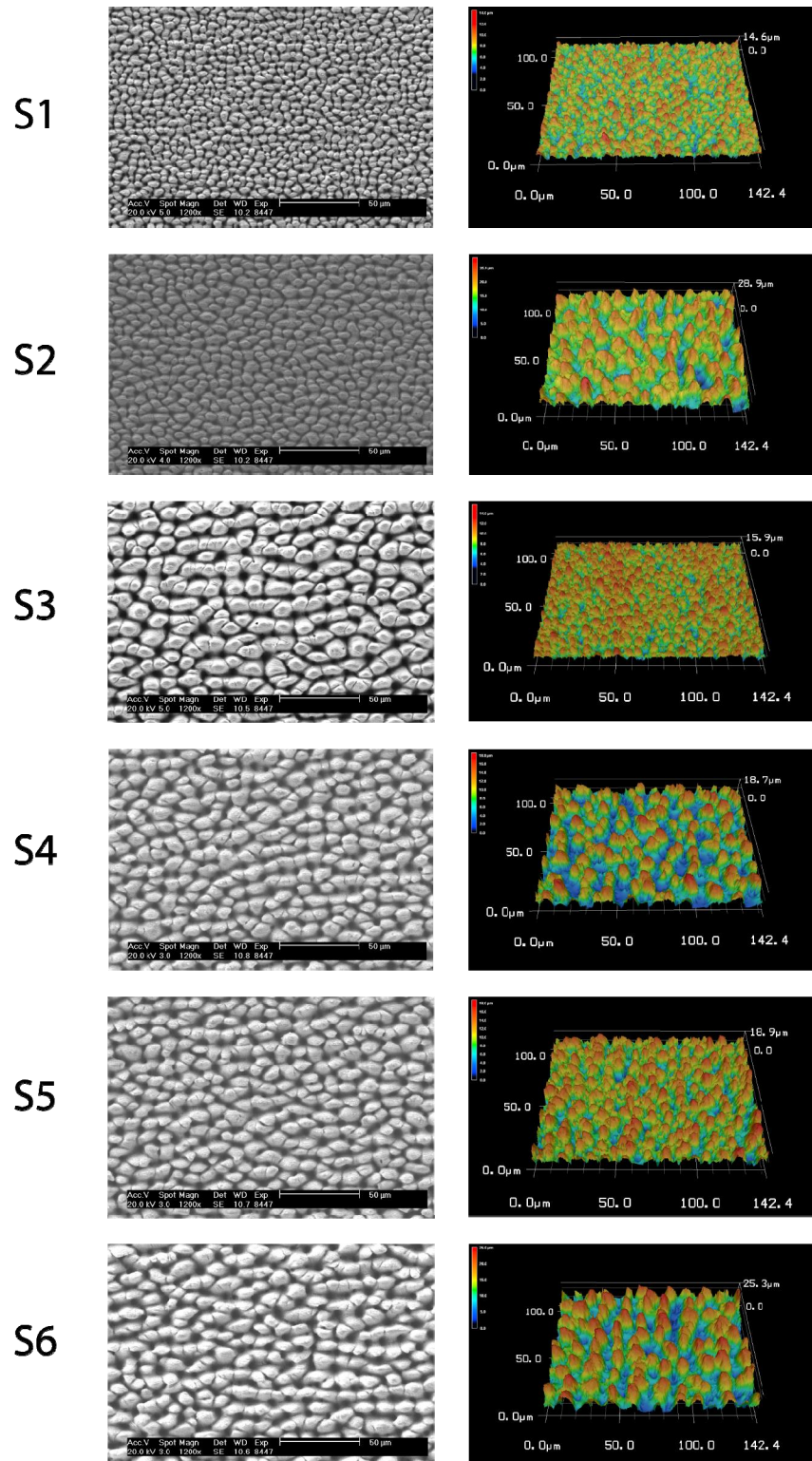


Figure 1: (Left) Scanning electron microscope (SEM) images and (Right) 3D surface profiles of laser-processed electrodes. The scale bar in the SEM images is 50 μm .

2.2 Electrolysis Efficiency

The electrochemical efficiency of each electrode surface during water splitting was characterized by measuring the current-voltage characteristics during the hydrogen evolution reaction (HER) in a 1 M potassium hydroxide (KOH) solution. The testing was performed using a custom-built acrylic 3-electrode electrolysis cell shown in Figure 2. In this configuration, the voltage is applied between the working electrode (the electrode under observation) and a reference electrode. This voltage then drives an electrochemical reaction in which the current is supplied by the counter electrode. In the present study, the reference electrode was CHInstruments Model 152 Hg/HgO electrode ($E^\circ = 0.85 \text{ V}$ at 25°C), which is shown in white in Figure 2. The counter electrode (the larger electrode in Figure 2) was 316 stainless measuring 2 inches by 4.4 inches and was processed with an area of 2 inches by 4 inches in order to ensure a sufficiently large enough surface area to not restrict current flow in the cell. The working (sample) electrodes were 1 inch by 2.5 inches in size, with a processed area of 1 inch by 2 inches. The use of the custom cell ensured that the relative positions between the 3 electrodes remained fixed for all experiments.

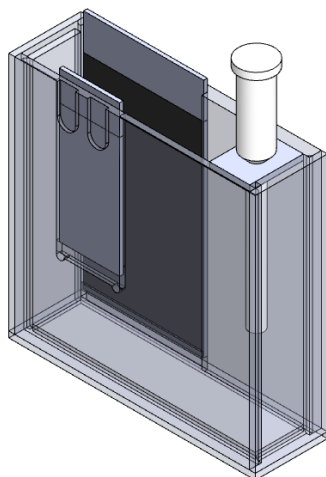


Figure 2: Isometric view of electrolysis cell used for current versus voltage experiments

3. RESULTS AND DISCUSSION

The electrochemical characteristics of the electrode surfaces are shown in Figure 3(a). The primary water-splitting reaction occurs for voltages below 1.2 V and is characterized by a linear Ohmic relationship. The slope of the current-voltage relationship is constant for all electrodes tested, which indicates that losses associated with the cell construction and the electrolyte were constant for all tests and therefore variations in performance can be attributed to differences between the electrodes under observation. The role of the microstructure separation can be most clearly seen by measuring the electrode potential as a function of microstructure separation for a constant current density of 0.05 A/cm^2 . At a constant current density, the rate of the electrochemical reaction and thus the quantity of hydrogen gas being evolved at the electrode surface is held constant. The voltage required to generate this current is then a direct measure of the electrode efficiency, with electrode efficiency being the highest for the electrode with the least negative voltage. This analysis is shown in Figure 3(b) and was generated using the surface properties listed in Table 1. The unprocessed electrode is plotted as having a mound separation of 0 as a reference for the performance of the laser-processed electrodes.

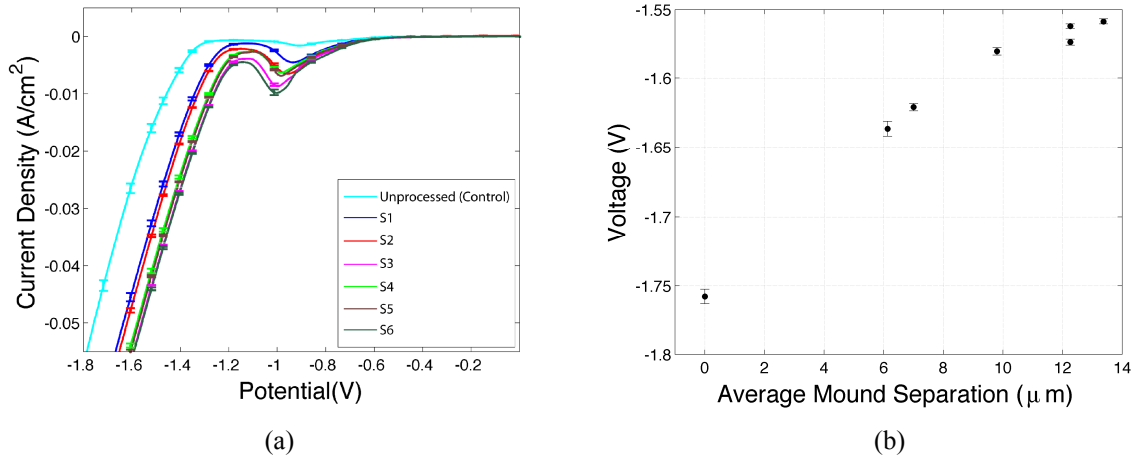


Figure 3: (a) Current vs Voltage plot of the hydrogen evolution reaction (HER) of laser-processed electrodes. (b) Electrode voltage relative to a Hg/HgO reference electrode as a function of mound spacing.

Figure 3(b) demonstrates that the efficiency of the electrodes increases nearly linearly with the average mound spacing over the range of separations tested. For the largest structure spacing tested, 13.4 microns, the overvoltage was reduced by 200 mV. Because the contact angle and the surface area of the electrodes are roughly constant for all of the laser-processed electrodes under observation, it is expected that the mechanism for the enhancement is related to the growth and release of bubbles on the electrode surface. Losses associated with the presence of gas bubbles can be attributed to two categories: the presence of bubbles in the electrolyte solution and the adhering of bubbles to the electrodes. In solution, bubbles increase the resistance and thus the cell loss. This loss can be minimized by careful design of the cell geometry, especially the separation distance between electrodes. This type of loss can be considered constant over the range of electrodes given the consistency of the current/voltage slopes (Figure 3(a)). On the electrode surface, bubbles shield a portion of the electrode and reduce the effective surface area, leading to increased current densities[10-14]. The production of gas on an electrode surface during an electrochemical reaction leads to a certain fraction of the electrode surface being covered by bubbles at any given time. This fraction (Θ) is referred to as the bubble coverage. The presence of bubbles necessitates a differentiation of the superficial current density (I/A) described by the total current (I) divided by the total electrode surface area (A), and the actual current density (j). The superficial and actual current densities are related by the equation:

$$j = \frac{I/A}{1 - \Theta} \quad (1)$$

Bubble coverage effectively decreases the active surface area and increases the actual current density associated with electrolysis in the remaining regions. A theoretical description of bubble formation on an electrode surface demonstrates that the bubble coverage depends on a variety of factors including the size of the bubbles released from the surface and bubble density [12]:

$$\Theta = \frac{\pi z}{2A} K_1^2 R_r^2; \quad K_1 = \begin{cases} 1 & \phi \leq 90^\circ \\ \sin(\phi) & \phi \geq 90^\circ \end{cases} \quad (2)$$

where (z/A) is the number of bubbles per area (A), K_1 takes into account the contact angle (ϕ) ($< 90^\circ$ for a hydrophilic surface), and R_r is the radius of bubbles right before release from the surface.

For a structured surface of the type seen in Figure 1, the surface geometry is able to influence the bubble coverage and thus the electrode efficiency by reducing the R_r , the radius of the released bubbles. It is expected that nucleation occurs in the valleys between microstructures on a rough surface. On a flat surface or a surface with steep, narrow structure separation (e.g. samples S1 and S2), a bubble will expand and cover an increasing portion of the surface until buoyancy forces or turbulence overcomes the adhesion of the bubble to the surface. When the distance between microstructures reaches approaches the widths of the structures themselves, the availability for contact between the growing bubble and the surface decreases. Instead, the bubble is gradually pushed out of the valley during growth and is expelled when the

bubble is only in contact with the peaks of the structures. This process by which the surface geometry can directly control R_r and by limiting surface contact is shown schematically in Figure 4.

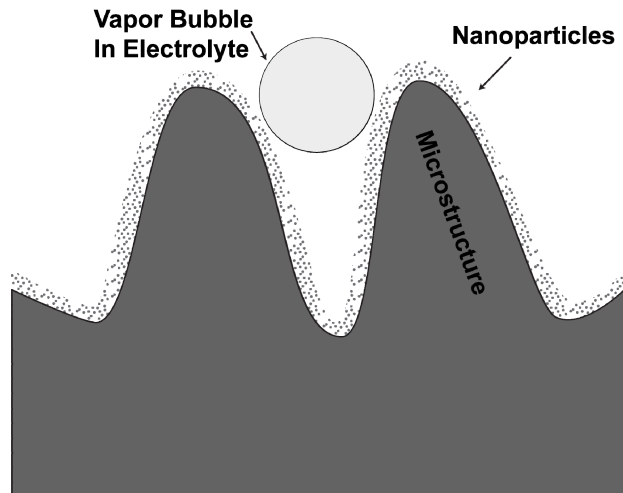


Figure 4: Schematic of vapor bubble formation during a phase transition on a multiscale surface.

Note that this physical mechanism is due to surface geometry and is a separate phenomenon than the wettability of the surface as measured by the bulk contact angle (related to K_1 in equation (2)). Thus, for a given surface area and contact angle, the efficiency of the hydrogen evolution reaction can be further tailored through the variation of the separation of the microscale structures as shown in Figure 3(b). Increasing the separation between microstructures reduces the contact between the vapor bubble and the electrode surface. This effect is further enhanced by the increased presence of circular pits with increasing mound separation as seen in the SEM images and 3D surface profiles in Figure 1.

ACKNOWLEDGEMENTS

This work has been supported by a Multi-University Research Initiative (MURI) No. – W911NF-06-1-0446 and a grant through the Nebraska Center for Energy Sciences Research (NCSR) with funds provided by Nebraska Public Power District (NPPD) to the University of Nebraska-Lincoln (UNL) No. 420000844.

4. CONCLUSION

The efficiency of the hydrogen evolution reaction (HER) associated with water splitting in an alkaline electrolysis cell was enhanced through the use of multiscale surface structures characterized by microscale mounds covered by nanoparticles. Specifically, overvoltage losses of up to 200 mV associated with bubble coverage on the electrode surfaces were mitigated by controlling the separation between the microscale surface structures. This enhancement is attributed to the specific role of surface geometry in promoting the efficient release of vapor bubbles from the electrode surface and is separate from the impacts of contact angle and surface area. The proposed technique towards the control of bubble production and release from a surface during phase transfer suggests a new pathway for increasing the efficiency of phase transfer not only in electrochemical applications, but also for heat transfer applications including nucleate boiling and condensation. The ability to fabricate functionalized surface structures directly on a metal also enhances the durability and permanency of such structures when utilized in extreme environments.

REFERENCES

- [1] C. A. Zuhlke, T. P. Anderson, and D. R. Alexander, "Formation of multiscale surface structures on nickel via above surface growth and below surface growth mechanisms using femtosecond laser pulses," *Opt. Express* 21(7), 8460–8473 (2013).

- [2] C. A. Zuhlke, T. P. Anderson, and D. R. Alexander, "Fundamentals of layered nanoparticle covered pyramidal structures formed on nickel during femtosecond laser surface interactions," *Applied Surface Science* 283, 648-653 (2013)
- [3] A. Y. Vorobyev and C. Guo, "Direct femtosecond laser surface nano/microstructuring and its applications," *Laser & Photon. Rev* 7, 385-407 (2012).
- [4] B. K. Nayak and M. C. Gupta, "Self-organized micro/nano structures in metal surfaces by ultrafast laser irradiation," *Optics and Lasers in Engineering* 48, 940-949 (2010)
- [5] C. A. Zuhlke, T. P. Anderson, and D. R. Alexander, "Comparison of the structural and chemical composition of two unique micro/nanostructures produced by femtosecond laser interactions on nickel," *Applied Physics Letters* 103, 121603-121603-5, (2013)
- [6] A.-M. Kietzig, S. G. Hatzikiriakos, and P. Englezos, "Patterned Superhydrophobic Metallic Surfaces," *Langmuir* 25(8), 4821-4827, (2009)
- [7] B. K. Nayak, M. C. Gupta, and K. W. Kolasinski, "Formation of nano-textured conical microstructures in titanium metal surface by femtosecond laser irradiation," *Appl. Phys. A* 90(3), 399-402 (2007).
- [8] A. Y. Vorobyev and C. Guo, "Metal pumps liquid uphill," *Applied Physics Letters* 94(22), 224102 (2009).
- [9] C. Kruse, T. P. Anderson, C. Wilson, C. Zuhlke, D. R. Alexander, G. Gogos, and S. Ndao, "Extraordinary Shifts of the Leidenfrost Temperature from Multiscale Micro/Nanostructured Surfaces," *Langmuir* 29(31), 9798-9806, (2013).
- [10] H. Vogt, "The limits of the analogy between boiling and gas evolution at electrodes," *International Journal of Heat and Mass Transfer* 47(4), 787-795 (2004).
- [11] H. Vogt and R. Balzer, "The bubble coverage of gas-evolving electrodes in stagnant electrolytes," *Electrochimica Acta* 50(10), 2073-2079 (2005).
- [12] J. Eigeldinger and H. Vogt, "The bubble coverage of gas-evolving electrodes in a flowing electrolyte," *Electrochimica Acta* 45(27), 4449-4456 (2000).
- [13] O. Teschke, "Effect of PTFE Coverage on the Performance of Gas Evolving Electrodes," *Journal of The Electrochemical Society* 131(5), 1095 (1984).
- [14] D. Kiuchi, H. Matsushima, Y. Fukunaka, and K. Kuribayashi, "Ohmic resistance measurement of bubble froth layer in water electrolysis under microgravity," *Journal of The Electrochemical Society* 153(8), E138-E143 (2006).